nature nanotechnology

ARTICLES

PUBLISHED ONLINE: 17 JULY 2011 | DOI: 10.1038/NNANO.2011.101

Cell-surface sensors for real-time probing of cellular environments

Weian Zhao[1,2,3,4], Sebastian Schafer[1,2,3,4], Jonghoon Choi[5], Yvonne J. Yamanaka[5,6], Maria L. Lombardi[7], Suman Bose[8], Alicia L. Carlson[2,9], Joseph A. Phillips[1,2,3,4], Weisuong Teo[1,2,3,4], Ilia A. Droujinine[1,2,3,4], Cheryl H. Cui[1,2,3,4], Rakesh K. Jain[10], Jan Lammerding[7], J. Christopher Love[5], Charles P. Lin[2,3,9], Debanjan Sarkar[1,2,3,4], Rohit Karnik[8] and Jeffrey M. Karp[1,2,3,4]*

The ability to explore cell signalling and cell-to-cell communication is essential for understanding cell biology and developing effective therapeutics. However, it is not yet possible to monitor the interaction of cells with their environments in real time. Here, we show that a fluorescent sensor attached to a cell membrane can detect signalling molecules in the cellular environment. The sensor is an aptamer (a short length of single-stranded DNA) that binds to platelet-derived growth factor (PDGF) and contains a pair of fluorescent dyes. When bound to PDGF, the aptamer changes conformation and the dyes come closer to each other, producing a signal. The sensor, which is covalently attached to the membranes of mesenchymal stem cells, can quantitatively detect with high spatial and temporal resolution PDGF that is added in cell culture medium or secreted by neighbouring cells. The engineered stem cells retain their ability to find their way to the bone marrow and can be monitored *in vivo* at the single-cell level using intravital microscopy.

Monitoring cell functions and cell-to-cell communication in the cellular environment has enormous implications for cell biology and regenerative medicine[1]. In the area of cell therapy there is also significant interest in better understanding and tracking the fate of transplanted cells[2,3]. Unfortunately, probing what cells 'see' and how they respond in real time to surrounding signals (i.e. cytokines) is still a major challenge[1]. Conventional assays, including flow cytometry, enzyme-linked immunosorbent assay (ELISA), immunostaining and polymerase chain reaction are valuable, but typically require stepwise staining, washing or manipulation before analysis. Alternative approaches include staining cells with metabolically and chemically engineered probes or nanoparticles[4–6]. However, most of these assays measure markers under 'static' conditions and fail to monitor what cells sense in real time, in a dynamic manner.

Fluorescence resonance energy transfer (FRET) sensors, particularly those using genetically engineered proteins, have offered a way to study protein expression, migration, conformational change and protein–protein interactions, as well as to probe metal ions and enzyme activities inside cells or on cell surfaces[6–10]. In addition, B cells have been engineered as sensors for the identification of pathogens; for example, a calcium-sensitive bioluminescent protein engineered onto cells emits light in the presence of pathogens[11]. Others have reported a luciferase-engineered cell approach that detects the local concentration of ATP at the cell surface[12]. However, these approaches require complex genetic engineering methods and cannot probe multiple markers simultaneously. Recently, the cell membrane has been engineered using chromatic polymer patches that produce light in the presence of cell-membrane-disrupting molecules[13]. Although useful for

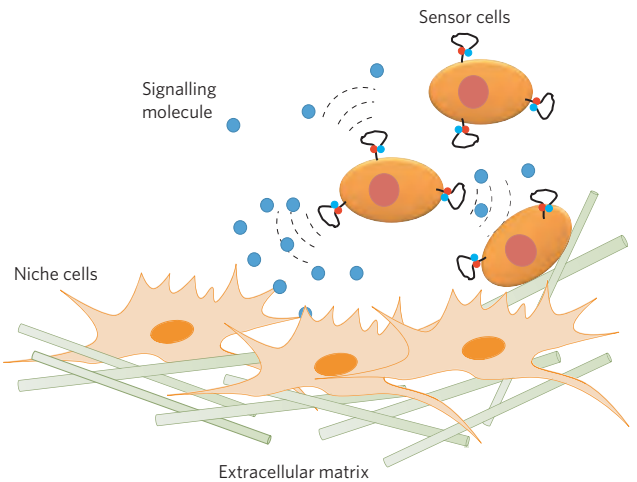

Scheme 1 | Probing the cellular niche environment and signalling using cells engineered with an aptamer sensor. Aptamer sensors that bind to signalling molecules (PDGF in this case) are covalently attached to the surface of cells (mesenchymal stem cells in this case). Signalling molecules secreted by niche cells are detected by the sensor cells, and the fluorescent signal generated is measured.

[1]Center for Regenerative Therapeutics & Department of Medicine, Brigham & Women's Hospital, 65 Landsdowne Street, Cambridge, Massachusetts 02139, USA, [2]Harvard Medical School, 65 Landsdowne Street, Cambridge, Massachusetts 02139, USA, [3]Harvard Stem Cell Institute, 65 Landsdowne Street, Cambridge, Massachusetts 02139, USA, [4]Harvard-MIT Division of Health Science and Technology, 65 Landsdowne Street, Cambridge, Massachusetts 02139, USA, [5]Department of Chemical Engineering, Massachusetts Institute of Technology, 77 Massachusetts Avenue, Cambridge, Massachusetts 02139, USA, [6]Department of Biological Engineering, Massachusetts Institute of Technology, 77 Massachusetts Avenue, Cambridge, Massachusetts 02139, USA, [7]Department of Medicine, Brigham and Women's Hospital/Harvard Medical School, 65 Landsdowne Street, Cambridge, Massachusetts 02139, USA, [8]Department of Mechanical Engineering, Massachusetts Institute of Technology, 77 Massachusetts Avenue, Cambridge, Massachusetts 02139, USA, [9]Wellman Center for Photomedicine and Center for Systems Biology, Massachusetts General Hospital/Harvard Medical School, 40 Blossom Street, Boston, Massachusetts 02114, USA, [10]Edwin L. Steele Laboratory, Department of Radiation Oncology, Massachusetts General Hospital/Harvard Medical School, 55 Fruit Street, Boston, Massachusetts 02114, USA. *e-mail: jkarp@rics.bwh.harvard.edu

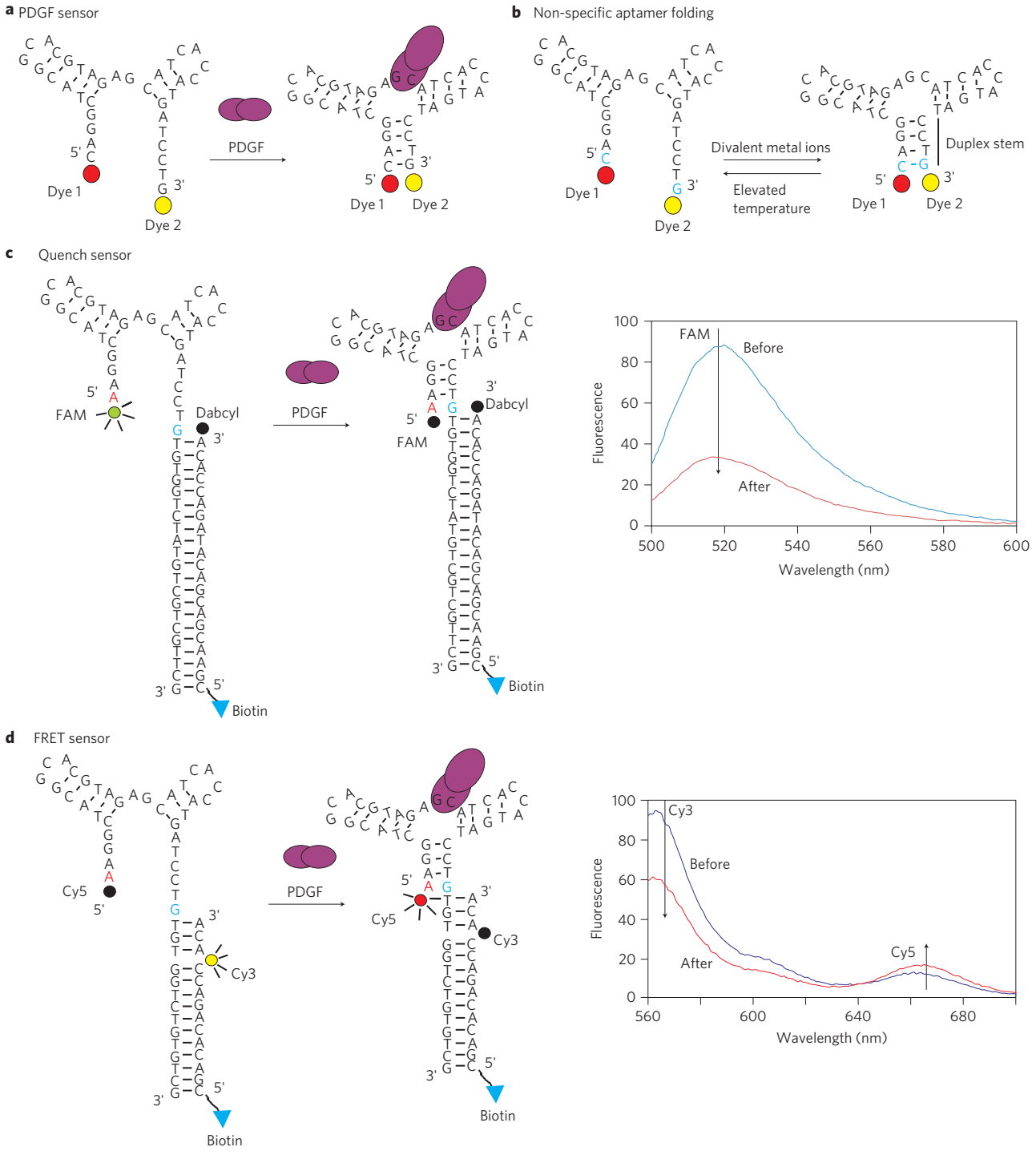

Figure 1 | Mechanism of PDGF aptamer sensors in solution. a, Original PDGF sensor described in ref. 28. When bound to PDGF, the aptamer changes from an open structure to a complex with paired bases in the stem region. The two dyes are located closer to one another and yield a fluorescent signal. **b**, Non-specific folding of the original sensor at elevated ionic strength in the presence of divalent metal ions. **c**,**d**, Engineered sensors. The terminal C–G base pair (blue) is mutated to an A–G pair (red–blue) for less non-specific folding in the aptamer. Biotin moieties allow immobilization on the cell surface. In the quench sensor (**c**), fluorescence of the FAM dye is quenched by a quencher molecule (Dabcyl) in the presence of 10 nM PDGF in PBS–/–. In the FRET sensor (**d**), donor dye (Cy3) fluorescence decreases and acceptor dye (Cy5) fluorescence increases upon addition of 10 nM PDGF in PBS. Spectra in **c** and **d** were recorded at room temperature.

predicting the cytotoxicity of molecules that perturb the cell membrane, this approach lacks potential for the general study of cell signalling.

In this Article, we present a simple, generic approach to using real-time probes at the cell surface for examining intercellular signalling within the cellular environment using nucleic acid aptamer sensors (Scheme 1). Specifically, we covalently attached fluorescent aptamer sensors to the surface of cells to produce a real-time signal when target molecule(s) contact the cell surface. Aptamers are single-stranded oligonucleotides that can be generated for a target molecule by an *in vitro* selection process (systematic evolution of ligands by exponential enrichment; SELEX) with

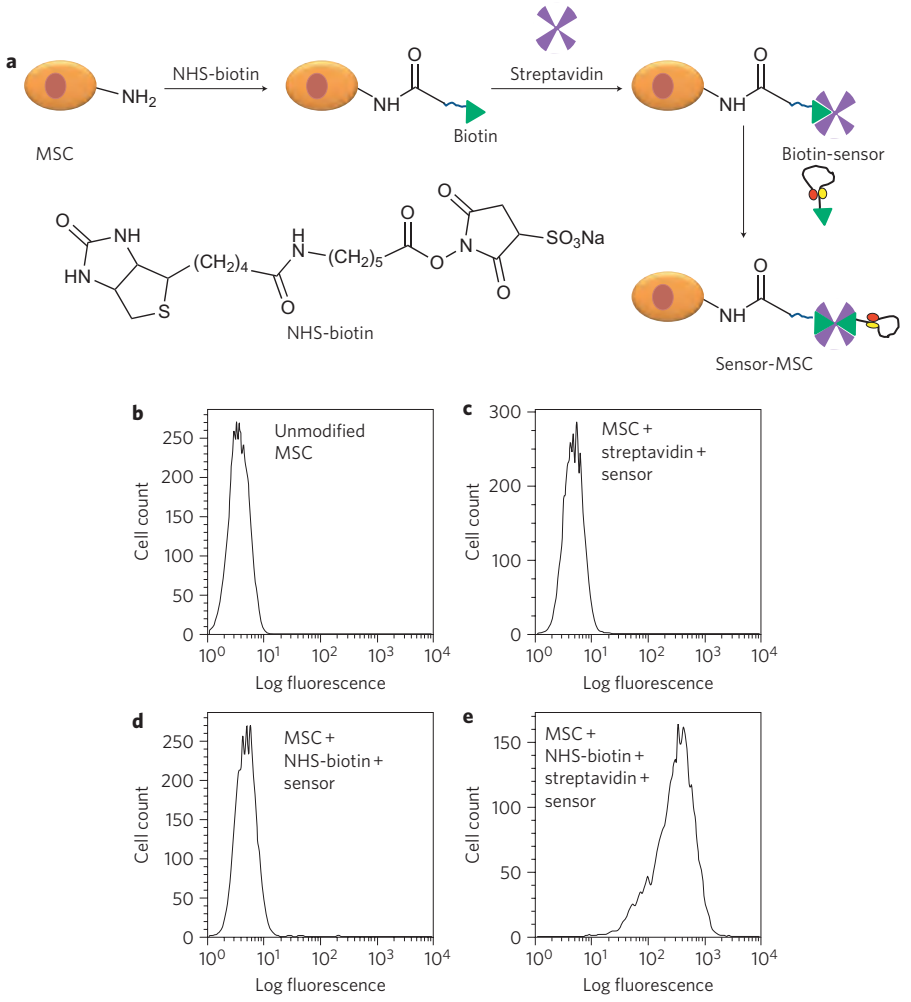

Figure 2 | Anchoring the engineered aptamer sensor to the cell surface. a, Schematic showing the chemistry approach used to attach sensors to MSCs. **b–e**, Flow cytometry data using the Cy3 signal of the FRET sensor show successful conjugation of the aptamer sensor on the cell surface.

high affinity[14–19]. Aptamers can be readily engineered for therapeutics or as probes for targeting, imaging or biosensing by introducing functional moieties including modified nucleotides, biotin or dyes during the chemical synthesis[16–22].

We have focused on attaching an aptamer that recognizes the platelet-derived growth factor (PDGF) onto the membrane of mesenchymal stem cells (MSCs). The use of MSCs is attractive because they can differentiate into different types of cells, including osteoblasts, adipocytes and chondroblasts, and they can promote angiogenesis and have immunomodulatory effects[2]. MSCs are currently being tested in over 100 clinical trials to regenerate damaged tissue and treat inflammation[2,23]. Although the clinical trials have met safety endpoints, some have recently failed to show efficacy[23] and this is attributed in part to an incomplete understanding of MSC biology, particularly how MSCs signal in their niche environment and communicate with other cells (i.e. endothelial cells, immune cells and cancer cells)[2,23]. We address this issue by constructing sensors for detecting PDGF, a potent chemoattractant that recruits MSCs to inflamed tissue and tumours, and an important signalling molecule in the participation of MSCs in vascular regeneration and communication with activated endothelial cells or tumour cells[24–26]. Importantly, PDGF aptamers and simple aptamer-based PDGF sensors have been described[27–29].

We envision that cell surface sensors can be delivered into a particular *in vivo* niche by means of delivery of an exogenous cell source. In particular, MSCs have been shown to home to sites of inflammation, bone marrow and to tumours[2]. Imaging of transplanted cells can then be achieved by intravital confocal microscopy (IVM), which has been used previously in the study of stem cell and leukocyte trafficking, cell functions and cell–cell interactions *in vivo*[1,30–32]. Through the combination of cell-surface sensors, cell homing and IVM, we hope the cell sensors can be used to study intercellular signalling and cellular microenvironments in real time, at single-cell resolution, in living animals.

Engineering aptamer sensors on the cell surface

A PDGF sensor based on a previously isolated aptamer sequence has already been engineered[27–29]. This PDGF sensor harnesses aptamer conformational changes that occur when binding to PDGF, which brings two attached dyes within close proximity; the crosstalk between the two dyes yields a fluorescence signal (Fig. 1a). This sensor is highly selective and detects PDGF in the picomolar range by producing an instantaneous signal[27,28]. However, these sensors were designed to operate in the solution phase and contain dyes at each end of the aptamer (Fig. 1a,b)[27,28]. To enable binding to the cell surface, we first engineered the aptamer sensor to have a surface anchoring moiety. As shown in Fig. 1c,d, the original single-stranded PDGF aptamer is extended at one end by a short oligonucleotide that can hybridize with its complementary strand (details of DNA sequences are provided in Supplementary Table S1). Two dyes, at desirable positions, and anchor moieties (i.e. biotin) can be accommodated easily on these

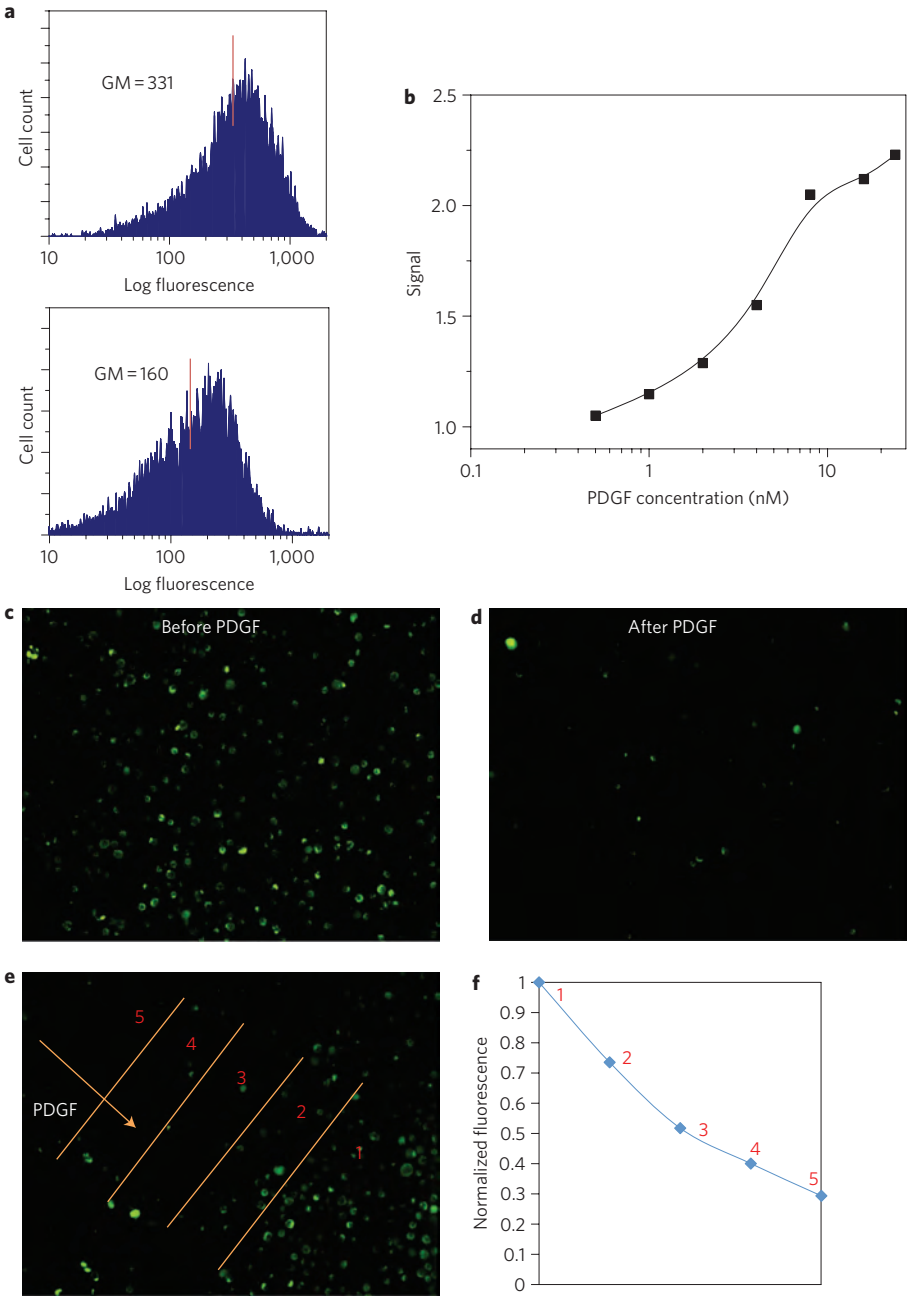

Figure 3 | Aptamer sensor functions on the cell surface. a, Representative sensor performance data, examined using flow cytometry, for the quench sensor immobilized on the MSC surface before and immediately after addition of 10 nM PDGF (GM, geometric mean). **b**, Sensor signal (defined as the ratio of GM before and after addition of PDGF) versus concentration of PDGF in PBS−/−. **c**,**d**, Representative fluorescent microscopy images of sensor cell before and immediately after addition of 10 nM PDGF in PBS−/−, respectively. **e**, PDGF (2 μM) was added to sensor-modified MSCs from the top/left corner (arrow shows direction) using a pipette tip, and the image was recorded immediately. **f**, The PDGF gradient was separated into five regions using image analysis, and the fluorescent intensities of 10 representative cells from each region were averaged and plotted. The sensor signal in region 1 is defined as 1; other regions are normalized accordingly.

two separated strands during DNA synthesis, and can then be annealed together before anchoring onto cells.

The original PDGF sensor developed by Tan's group undergoes non-specific folding that occurs in the presence of divalent metal ions (i.e. Mg^{2+} and Ca^{2+}) and thus produces a high background, making it unsuitable for physiological conditions (Fig. 1b)[27,28]. To overcome this issue, we mutated the aptamer sequence by changing a C–G base pair in the stem to an A– –G non-base pair. Such a mutation and the above-mentioned two-stranded sensor design did not significantly impair the aptamer binding ability. We engineered two types of sensors: a quench sensor (FAM/Dabcyl) (Fig. 1c) and a FRET sensor (Cy3/Cy5) (Fig. 1d). The sensors showed robust performance in the presence of divalent metal ions (phosphate buffered saline, PBS + /+) (Supplementary Fig. S1). Note also that a temperature change (in the range from room temperature to 37 °C) does not have a significant impact on the binding affinity of the aptamer to PDGF; rather, an elevated temperature (i.e. 37 °C) disrupts the duplex stem and drives the equilibrium to the unfolded state in the absence of PDGF, which therefore produces a higher (beneficial) signal-to-noise ratio (Fig. 1b and data not shown).

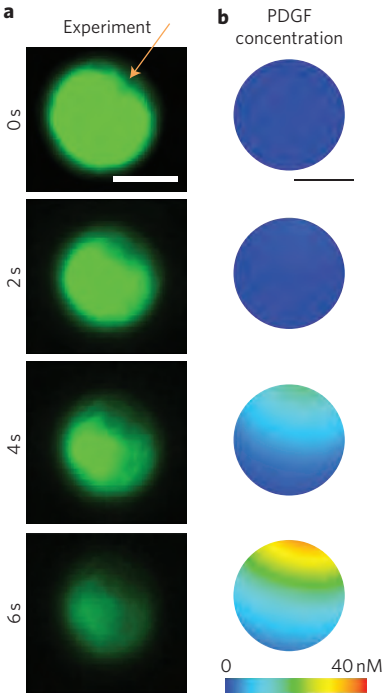

Figure 4 | Spatial-temporal imaging of a single MSC functionalized with the quench sensor demonstrates that PDGF sensing correlates with data generated from a computational model. a, PDGF (2 μM) was injected 30 μm from the cell using a microneedle, as indicated by the orange arrow (Supplementary Fig. S5 includes a representative light microscope image showing the microneedle juxtaposed to the cell surface). The signal was quenched as PDGF engaged the sensor while moving across the cell surface as a function of time, as observed by fluorescent microscopy. **b**, Concentration of PDGF on the cell surface as predicted from a three-dimensional computational mass transport model (described in Supplementary Information). Scale bar, 10 μm.

The simple chemistry approach of attaching sensors on the cell membrane bypasses the complex genetic, enzymatic or metabolic engineering approaches used previously for modifying the cell surface. Specifically, our cell modification procedure consists of three steps involving treating cell surface amines with sulphonated biotinyl-*N*-hydroxy-succinimide (NHS–biotin), followed by streptavidin–biotin interactions (Fig. 2)[33,34]. Previously, using dye-conjugated molecules and flow cytometry, we showed that the cell surface coverage (of biotin, streptavidin or target ligand) at each step can be controlled by adjusting the reagent concentration and reaction times during conjugation[35] (D. Sarkar *et al.*, data not shown). Approximately 21,000 molecules are typically attached on each MSC (D. Sarkar *et al.*, data not shown). This method for functionalizing the surface and the presence of ligands on the cell surface did not affect the cell phenotype or homing ability[33–35] (D. Sarkar *et al.*, unpublished observations).

The quench sensor (Fig. 1c) functioned well on the cell surface, and the addition of PDGF resulted in a decrease in fluorescence (Fig. 3). Sensors on the cell surface respond to PDGF within seconds; the sensor signal quantitatively correlates with the concentration of PDGF added into the cell solution (Fig. 3b) and is specific to PDGF (Supplementary Fig. S2). Because the quench sensor does not have an internal reference and the signal may be influenced by external factors (including sensor site density and medium conditions), the FRET sensor (Fig. 1d) was also used to quantitatively detect PDGF. The non-specific background signal is minimized in this case because the signal produced is based on the ratio of decreased Cy3 fluorescence and increased Cy5 fluorescence (Supplementary Fig. S3). Moreover, the detection range of sensors on the cell surface spans from several hundred pM to low nM levels, which is within the range of serum PDGF concentrations (400–700 pM under physiological conditions, or higher under pathological conditions such as tumours)[36,37]. Data from both the quench sensor and the FRET sensor in different culture media (PBS−/−, PBS+/+ and MSC medium with 15% fetal bovine serum (FBS)) are presented in Supplementary Fig. S4.

Spatial-temporal sensing using sensor-engineered cells

To determine whether sensors on cells produce a fluorescence signal in real time that can be resolved with high spatial resolution at the single-cell level, PDGF was added in close proximity to the cells though a micromanipulator-mounted microneedle coupled to a microinjector (Supplementary Fig. S5). Fluorescence imaging showed spatial variation of the signal intensity over the cell surface, which evolved over time as more PDGF was transported by the impinging flow to the cell surface (Fig. 4a). We also simulated the evolution of PDGF concentration in the vicinity of a cell using a three-dimensional unsteady convection–diffusion mass transport model (described in the Supplementary Information and Fig. S6). The evolution of PDGF concentrations on the surface of the cell was consistent with the observed fluorescence quenching behaviour; the model predicted a transition of the PDGF concentration in the vicinity of the cell from 0 nM at $t = 0$ to 40 nM at $t = 6$ s (Fig. 4b). Given that this aptamer sensor, when attached on the cell surface, detects PDGF in the range of ~1–10 nM (Fig. 3b), the timescale of a cell response is consistent with the timescale required for the PDGF concentration to change.

The development of sensors that can be used to examine cell-to-cell communication in real time at a single-cell level is invaluable for elucidating mechanisms of intercellular communication. Based on a microwell assay developed by Love and co-workers[38], we show that our sensor MSCs can detect PDGF secreted by neighbouring cells. On a polymeric substrate containing an array of microwells, we added sensor-modified MSCs and PDGF-producing MDA-MB-231 cells[39] (PDGF production was confirmed and quantified by ELISA; see Supplementary Methods). Cells settle by gravity into the microwells, which contain subnanolitre volumes (0.1 nl) with different combinations of cell ratios (sensor MSC:PDGF-producing MDA-MB-231 cells = 1:0, 1:1, 1:2, 1:3+; Fig. 5). The fluorescence signal of the sensor MSCs was imaged continuously over time (6 h) as PDGF was produced by the MDA-MB-231 cell. As shown in Fig. 5, sensors on the MSC surface indeed produced a fluorescence signal that correlated directly with the number of MDA-MB-231 cells in the same microwell with the sensor MSC. In contrast, no significant signal difference was observed in the sensor signal when sensor MSCs were incubated alone or with native MDA-MB-231 cells (not engineered to secrete PDGF; Supplementary Fig. S7).

In vivo monitoring of sensor-engineered cells

As a first step towards using cell surface sensors to monitor the cellular environment, cell function and intercellular signalling *in vivo*, we tested the feasibility of using IVM to monitor the engineered cells after transplantation. To examine if aptamer conjugation affects the natural homing ability of MSC to bone marrow, both native and aptamer–MSC were injected simultaneously into Balb/c mice, and bone marrow imaging was performed 24 h post-injection[40]. Using a fluorescence confocal and multiphoton intravital imaging system that tracks single cells in living animals, we observed ~30 cells per image stack for both sensor-engineered MSCs and native MSCs (Fig. 6a,b,c). The transendothelial migration of aptamer–MSC and unmodified MSC was not statistically different, $P = 0.116$ (Fig. 6d).

Given that the FRET system is desirable for *in vivo* studies as it provides a ratio of two distinct fluorescent dyes, thereby minimizing

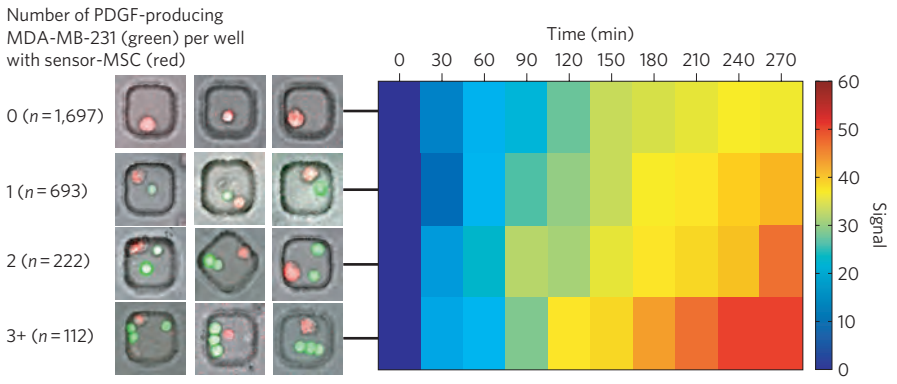

Figure 5 | Real-time sensing of PDGF secretion from neighbouring MDA-MB-231 cells by sensor-engineered MSCs. Left panel: representative images of microwells containing different numbers of PDGF-producing MDA-MB-231 cells (green) in the same well with sensor MSC (red) at time $t = 0$ (n is the number of MSCs used in the analysis). MDA-MB-231 is genetically engineered to secrete PDGF that is fused with a GFP tag. To be distinguishable, the quench sensor in this set of experiments is labelled with a red dye (Cy5), and with Iowa Black RQ as a quencher. Cy5/Iowa Black RQ and FAM/Dabcyl perform similarly (Supplementary Fig. S9). Right panel: fluorescence of sensor MSC declining during the course of PDGF production. The signal, which is defined as the percentage of MSCs that have fluorescence intensity less than 50% of their initial value at the indicated time, correlates with the number of PDGF-producing MDA-MB-231 cells in the same well as a sensor MSC.

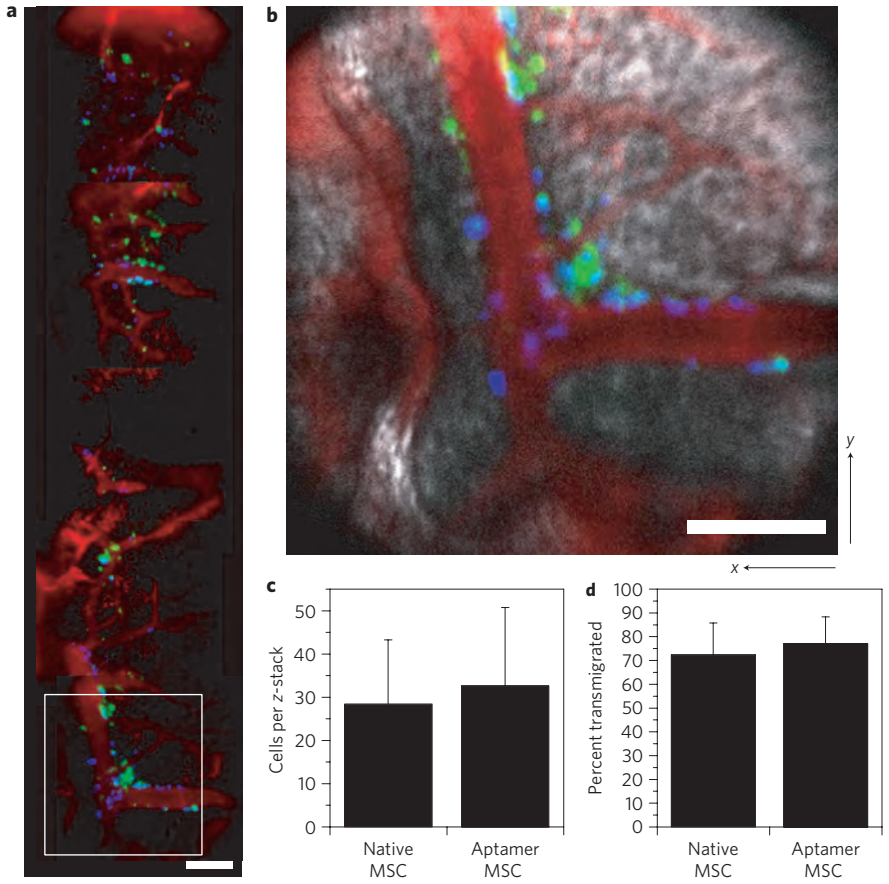

Figure 6 | Bone marrow homing and transmigration of aptamer-labelled MSCs. a, Large-area map of right parietal bone marrow compartments in an eight-week-old Balb/c mouse 24 h after injection of MSC and aptamer-MSC. Several image stacks were acquired in the right parietal bone ~200 μm to the right of the sagittal suture. **b**, Zoomed-in image of the area in the white box in **a**, shows a similar distribution of MSC (green) and aptamer-MSC (blue) in the vicinity of a large venule (red). **c**, Quantification of the average number of cells per z-stack. **d**, Quantification of percentage of cells positioned outside blood vessels shows no difference between MSC and aptamer-MSC (P-value = 0.116). MSC, green; aptamer-MSC, blue; blood vessels, red; bone, white. Scale bar, 100 μm.

the non-specific background signal, we designed a simple oligonucleotide (FRET-probe, Supplementary Table S1) to address whether we could sense a change in FRET signal in a live mouse. The FRET probe carries Cy3 and Cy5 in close proximity, which initially projects a Cy5 signal when exciting Cy3. To examine if the FRET probe was viable in bone marrow *in vivo* (a key

requirement for our sensor to work), we performed acceptor photobleaching of the Cy5 moiety *in situ* using a 635 nm laser, and a switch from Cy5 (red) to Cy3 (green) signal resulted (Supplementary Fig. S8). This experiment clearly suggests that it is feasible to use IVM to track transplanted sensor-engineered cells and monitor their signalling with the target molecules in their *in vivo* niche environment.

Conclusions

We have developed a simple cell-surface sensor platform that permits signalling to be monitored within the cellular environment, in real time, *in vitro* and potentially *in vivo*. Aptamer sensors can be readily modified with sensing molecules and surface anchors, and the binding affinity, folding and secondary structures can be engineered by mutating the aptamer sequences (Fig. 1)[41]. Furthermore, aptamer sensors for a large variety of target molecules can be obtained using (automated) SELEX[14–20,42,43]. We have shown that MSCs engineered with an aptamer can be detected in mouse bone marrow by IVM 24 h post-transplantation, and the communication between FRET dyes is retained, suggesting that nucleic-acid-sensor conjugated fluorophores are functional on the cell surface for at least one day under physiological conditions. If required, nucleic acid stability towards nuclease degradation *in vivo* can be improved without impairing the binding affinity and signalling performance by incorporating protecting groups such as poly(ethylene glycol) (PEG), phosphorothioates and locked nucleic acids[41].

We are currently engineering a reversible 'structure switching'[44,45] PDGF aptamer that has a covalent linker and complementary DNA (cDNA) that will compete with PDGF binding. Through this approach, when the PDGF concentration decreases, the bound PDGF, which is in competition with the cDNA, will dissociate quickly, allowing the rise and fall of signals to be monitored in real time.

Our cell surface sensors can be resolved spatiotemporally at the single-cell level (Fig. 4) and this is significant because cells respond to cues in their microenvionment in both time and space[46]. Furthermore, the sensor could respond quantitatively to PDGF added to the culture medium or secreted by adjacent cells. This is useful for reporting on the state of cell signalling under physiological or pathological conditions such as inflammation. The 49 mer PDGF sensor sequence used in this study is ~16 nm when fully stretched in a duplex format[47], and is expected to adopt a three-dimensional, tertiary structure upon binding to PDGF, leading to a dynamic radius less than ~8 nm. At this scale, the aptamer sensors sense signalling molecules at or near the cell surface. Note also that the local cytokine concentration in the vicinity of the cell surface is often distinct from the bulk medium because of delayed diffusion due to unstirred layer effects or degradation by cell-surface enzymes[48]. Our approach may therefore provide significant advantages over traditional *in vitro* techniques (such as ELISA) that can only assess bulk concentration of cytokines, and may serve as a new tool to quantitatively measure signalling molecules or potentially drugs at the cell surface with high spatiotemporal resolution under physiological conditions.

Our long-term goal is to use the natural homing ability of specific cell types to deliver sensors to particular niches (such as bone marrow, lymph nodes, inflamed tissue or tumours) to monitor intercellular communication in real time *in vivo*. Cell homing is a specific and highly regulated, multistep process that includes cell rolling, adhesion and transendothelial migration and is mediated by specific receptor–ligand interactions[2]. Direct placement of sensors into such environments would otherwise not be feasible without an invasive approach that may affect cell signalling. An important component of our approach is the use of IVM to monitor single cells in real time in living animals, and at a temporal and spatial resolution that is not presently possible with other techniques[1,30–32].

Previously, we and others have applied IVM to study the trafficking of leukocytes, haematopoietic stem cells and MSCs[31,32] (D. Sarkar *et al.*, unpublished observations). In such studies, cells are typically labelled with lipophilic dyes or fluorescent proteins that can 'passively' indicate the location of a cell, but cannot report the phenotype or the properties that define the cellular microenvironment. In contrast, the cell-surface sensor approach makes use of functional aptamer sensors that dynamically monitor intercellular signalling in real time. Our ongoing work focuses on further engineering our FRET sensor to have a high signal-to-noise ratio under physiological conditions to monitor PDGF levels produced in the MSC niche by activated endothelial cells, tumour cells or in response to injury. In our experience, a signal-to-noise ratio of >4 is required for *in vivo* imaging. This work will ultimately lead to a better understanding of MSC biology, particularly in PDGF-signalling, including tissue regeneration, angiogenesis, immunomodulatory and tumour modelling[24–26].

Finally, chemistry-based cell engineering approaches have recently been developed to study cell-immobilized signalling moieties both *in vitro* and *in vivo* in living animals[4,5,49]. For example, Bertozzi *et al.* reported the labelling of fluorophores on glycans using click chemistry in zebrafish, which permitted them to visualize glycan expression *in vivo*[4]. It is conceivable that in addition to labelling exogenous transplanted cells, the site-specific labelling of endogenous cells with 'sensing molecules' may become a valuable tool with which to monitor physiological and pathological changes *in vivo*. We anticipate that our study will serve as a gateway for the future development of a large toolkit of cell-surface sensors that biologists could routinely apply to elucidate cell biology both *in vitro* and *in vivo*.

Methods

Engineering aptamer sensors onto the MSC surface. MSCs (~1 M after trypsinization) (see Supplementary Information for routine MSC culture) were dispersed in biotin–NHS solution (1 mM in PBS−/−, 1 ml), and the solution was allowed to incubate for 10 min at room temperature. After washing, streptavidin solution (50 μg ml^{-1} in PBS−/−, 1 ml) was then used to treat the cells for 5 min. Finally, biotin-modified sensor solution (two DNA strands were first annealed at 5 μM each in PBS + /+ at 90 °C for 3 min and cooled at room temperature for 30 min, 200 μl) was added, and the suspension was incubated for 5 min at room temperature. The cells were then washed once by PBS−/− and subsequently used for experimentation. The fluorescent nature of the sensors allowed the conjugation step to be easily followed by flow cytometry (BD FACS Calibur flow cytometer) then analysed using Cell Quest software.

Microneedle experiment. Microneedle experiments were performed using a microinjector (FemtoJet, Eppendorf) with Eppendorf Femtotips and an Eppendorf micromanipulator (InjectMan NI 2, Eppendorf) (Supplementary Fig. S5). Glass microneedles with inner tip diameters of ~3 μm were made using a micropipette puller (P-97 Sutter Instrument Company). Microneedles were backfilled with the PDGF (2 μM in PBS−/−) using Eppendorf Femtotips Capillary Pipet Tips Microloaders. The microneedle, controlled by a micromanipulator, was lowered onto a dish with sensor-engineered MSCs settled on the surface in PBS−/−, positioned at a defined lateral distance (~40 μm) from the settled cells and at a height of ~30 μm from the underlying substrate. PDGF was released from the micropipette by applying a defined pressure (26 hPa). Simultaneously, phase contrast and fluorescence images of the cells were collected sequentially with a 1 s interval exposure time. Between 10 and 12 cells were measured in each experiment.

Computational model for PDGF transport in microneedle experiment. See Supplementary Information.

Cell–cell communication microwell assay and analysis. Time-course microwell assays were performed following previously reported protocols with some modifications[38]. The fabrication of the microwell is presented in the Supplementary Information. A sensor MSC suspension (1×10^5 cells/ml) was first placed on the surface of the array and cells were permitted to settle into the microwells by gravity. After 2 min, excess cells were washed away with serum-free media. Next, PDGF-producing MDA-MB-231 cells (1×10^5 cells/ml) in medium containing 15% FBS were loaded into the wells as described above. After a brief incubation at 37 °C with 5% CO_2, the array was delivered to the microscope for imaging. All images were acquired on an automated inverted fluorescence microscope (Zeiss Observer Z-1, Carl Zeiss Inc.) equipped with a stage incubator (PM S1) and incubation chamber for live-cell imaging (37 °C, 5% CO_2). Phase and fluorescence (GFP and Cy5)

micrographs were collected every 3 min for 6 h. A total of ~3000 microwells were imaged at each time point. A custom-written image analysis program was used to identify the location and fluorescence intensity of each cell in the microwell array, as described previously[38]. A MATLAB script was written to track the fluorescence signal intensity of each sensor MSC over the 6 h time course. The signal intensity of each sensor MSC was normalized to the signal intensity at $t = 0$ min to account for the baseline cell-to-cell variation in sensor MSC intensity. Sensor MSCs were divided into groups based on the number of PDGF-producing MDA-MB-231 cells residing in the same microwell (0, 1, 2 or 3+). More than 100 MSCs (see Fig. 5 for exact numbers) from each group were tracked. The fraction of sensor MSCs in each group with signal intensity less than 50% of the initial signal intensity was calculated at each time point.

Animals and intravital confocal microscopy. See Supplementary Information.

Received 3 December 2010; accepted 2 June 2011; published online 17 July 2011

References

1. Halin, C., Mora, J., Sumen, C. & von Andrian, U. *In vivo* imaging of lymphocyte trafficking. *Annu. Rev. Cell. Dev. Biol.* **21,** 581–603 (2005).
2. Karp, J. M. & Teo, G. Mesenchymal stem cell homing: the devil is in the details. *Cell Stem Cell* **4,** 206–216 (2009).
3. Ferreira, L., Karp, J. M., Nobre, L. & Langer, R. New opportunities: the use of nanotechnologies to manipulate and track stem cells. *Cell Stem Cell* **3,** 136–146 (2008).
4. Laughlin, S. T., Baskin, J. M., Amacher, S. L. & Bertozzi, C. R. *In vivo* imaging of membrane-associated glycans in developing zebrafish. *Science* **320,** 664–667 (2008).
5. Cook, B. N. & Bertozzi, C. R. Chemical approaches to the investigation of cellular systems. *Bioorg. Med. Chem.* **10,** 829–840 (2002).
6. Giepmans, B. N. G., Adams, S. R., Ellisman, M. H. & Tsien, R. Y. The fluorescent toolbox for assessing protein location and function. *Science* **312,** 217–224 (2006).
7. Hoffmann, C. *et al.* A FlAsH-based FRET approach to determine G protein-coupled receptor activation in living cells. *Nature Methods* **2,** 171–176 (2005).
8. Pollok, B. A. & Heim, R. Using GFP in FRET-based applications. *Trends Cell Biol.* **9,** 57–60 (1999).
9. Modi, S. *et al.* A DNA nanomachine that maps spatial and temporal pH changes inside living cells. *Nature Nanotech.* **4,** 325–330 (2009).
10. Albizu, L. *et al.* Time-resolved FRET between GPCR ligands reveals oligomers in native tissues. *Nature Chem. Biol.* **6,** 587–594 (2010).
11. Rider, T. *et al.* A B cell-based sensor for rapid identification of pathogens. *Science* **301,** 213–215 (2003).
12. Beigi, R., Kobatake, E., Aizawa, M. & Dubyak, G. Detection of local ATP release from activated platelets using cell surface-attached firefly luciferase. *Am. J. Physiol. Cell Physiol.* **276,** C267–C278 (1999).
13. Orynbayeva, Z. *et al.* Visualization of membrane processes in living cells by surface-attached chromatic polymer patches. *Angew. Chem. Int. Ed.* **44,** 1092–1096 (2005).
14. Tuerk, C. & Gold, L. Systematic evolution of ligands by exponential enrichment: RNA ligands to bacteriophage T4 DNA polymerase. *Science* **249,** 505–510 (1990).
15. Ellington, A. & Szostak, J. *In vitro* selection of RNA molecules that bind specific ligands. *Nature* **346,** 818–822 (1990).
16. Liu, J., Cao, Z. & Lu, Y. Functional nucleic acid sensors. *Chem. Rev.* **109,** 1948–1998 (2009).
17. Zhao, W., Brook, M. & Li, Y. Design of gold nanoparticle based colorimetric biosensing assays. *ChemBioChem* **9,** 2363–2371 (2008).
18. Sefah, K. *et al.* Nucleic acid aptamers for biosensors and bio-analytical applications. *Analyst* **134,** 1765–1775 (2009).
19. Nutiu, R. & Li, Y. *In vitro* selection of structure-switching signaling aptamers. *Angew. Chem. Int. Ed.* **44,** 1061–1065 (2005).
20. Keefe, A. D., Pai, S. & Ellington, A. Aptamers as therapeutics. *Nature Rev. Drug Discov.* **9,** 573–550 (2010).
21. Fang, X. & Tan, W. Aptamers generated from cell-SELEX for molecular medicine: a chemical biology approach. *Acc. Chem. Res.* **43,** 48–57.
22. Dhar, S., Kolishetti, N., Lippard, S. J. & Farokhzad, O. C. Targeted delivery of a cisplatin prodrug for safer and more effective prostate cancer therapy *in vivo*. *Proc. Natl Acad. Sci. USA* **108,** 1850–1855.
23. Ankrum, J. & Karp, J. M. Mesenchymal stem cell therapy: two steps forward, one step back. *Trends Mol. Med.* **16,** 203–209 (2010).
24. López Ponte, A. *et al.* The *in vitro* migration capacity of human bone marrow mesenchymal stem cells: comparison of chemokine and growth factor chemotactic activities. *Stem Cells* **25,** 1737–1745 (2007).
25. Beckermann, B. *et al.* VEGF expression by mesenchymal stem cells contributes to angiogenesis in pancreatic carcinoma. *Br. J. Cancer* **99,** 622–631 (2008).
26. Ball, S. G., Shuttleworth, C. A. & Kielty, C. M. Mesenchymal stem cells and neovascularization: role of platelet-derived growth factor receptors. *J. Cell. Mol. Med.* **11,** 1012–1030 (2007).
27. Fang, X., Sen, A., Vicens, M. & Tan, W. Synthetic DNA aptamers to detect protein molecular variants in a high-throughput fluorescence quenching assay. *ChemBioChem* **4,** 829–834 (2003).
28. Vicens, M., Sen, A., Vanderlaan, A., Drake, T. & Tan, W. Investigation of molecular beacon aptamer-based bioassay for platelet-derived growth factor detection. *ChemBioChem* **6,** 900–907 (2005).
29. Green, L. S. *et al.* Inhibitory DNA ligands to platelet-derived growth factor B-chain. *Biochemistry* **35,** 14413–14424 (1996).
30. Adams, G. B. *et al.* Haematopoietic stem cells depend on Gα(s)-mediated signalling to engraft bone marrow. *Nature* **459,** 103–107 (2009).
31. Lo Celso, C. *et al.* Live-animal tracking of individual haematopoietic stem/progenitor cells in their niche. *Nature* **457,** 92–97 (2009).
32. Lo Celso, C., Wu, J. W. & Lin, C. P. *In vivo* imaging of hematopoietic stem cells and their microenvironment. *J. Biophoton.* **2,** 619–631 (2009).
33. Sarkar, D. *et al.* Chemical engineering of mesenchymal stem cells to induce a cell rolling response. *Bioconjug. Chem.* **19,** 2105–2109 (2008).
34. Sarkar, D. *et al.* Engineered mesenchymal stem cells with self-assembled vesicles for systemic cell targeting. *Biomaterials* **31,** 5266–5274 (2010).
35. Zhao, W. *et al.* Mimicking the inflammatory cell adhesion cascade by nucleic acid aptamer programmed cell–cell interactions. *FASEB J.* doi:10.1096/fj.10-178384 (2011).
36. Lai, R. Y., Plaxco, K. W. & Heeger, A. J. Aptamer-based electrochemical detection of picomolar platelet-derived growth factor directly in blood serum. *Anal. Chem.* **79,** 229–233 (2007).
37. Leitzel, K. *et al.* Elevated plasma platelet-derived growth factor B-chain levels in cancer patients. *Cancer. Res.* **51,** 4149–4154 (1991).
38. Ogunniyi, A. O., Story, C. M., Papa, E., Guillen, E. & Love, J. C. Screening individual hybridomas by microengraving to discover monoclonal antibodies. *Nature Protoc.* **4,** 767–782 (2009).
39. Au, P. *et al.* Paradoxical effects of PDGF-BB overexpression in endothelial cells on engineered blood vessels *in vivo*. *Am. J. Pathol.* **175,** 294–302 (2009).
40. Mazo, I. B. *et al.* Hematopoietic progenitor cell rolling in bone marrow microvessels: parallel contributions by endothelial selectins and vascular cell adhesion molecule 1. *J. Exp. Med.* **188,** 465–474 (1998).
41. Jayasena, S. Aptamers: an emerging class of molecules that rival antibodies in diagnostics. *Clin. Chem.* **45,** 1628–1650 (1999).
42. Cox, J. C., Rudolph, P. & Ellington, A. D. Automated RNA selection. *Biotechnol. Prog.* **14,** 845–850 (1998).
43. Lou, X. *et al.* Micromagnetic selection of aptamers in microfluidic channels. *Proc. Natl Acad. Sci. USA* **106,** 2989–2994 (2009).
44. Kim, G., Kim, K., Oh, M. & Sung, Y. The detection of platelet derived growth factor using decoupling of quencher-oligonucleotide from aptamer/quantum dot bioconjugates. *Nanotechnology* **20,** 175503 (2009).
45. Tang, Z. *et al.* Aptamer switch probe based on intramolecular displacement. *J. Am. Chem. Soc.* **130,** 11268–11269 (2008).
46. Hui, E. & Bhatia, S. Micromechanical control of cell–cell interactions. *Proc. Natl Acad. Sci. USA* **104,** 5722–5726 (2007).
47. Zhao, W., Gao, Y., Kandadai, S. A., Brook, M. A. & Li, Y. DNA polymerization on gold nanoparticles through rolling circle amplification: towards novel scaffolds for three-dimensional periodic nanoassemblies. *Angew. Chem. Int. Ed.* **45,** 2409–2413 (2006).
48. Hayashi, S., Hazama, A., Dutta, A. K., Sabirov, R. Z. & Okada, Y. Detecting ATP release by a biosensor method. *Sci. STKE* **2004,** pl14 (2004).
49. Zhao, W., Teo, G., Kumar, N. & Karp, J. Chemistry and material science at the cell surface. *Mater. Today* **13,** 14–21 (2010).

Acknowledgements

The authors thank Lei Xu and Dannie Wang for the preparation of PDGF-producing MDA-MB-231 cells. This work was supported by the National Institutes of Health (NIH; grants nos. HL097172, HL095722 and DE019191 to J.M.K., grants nos. HL082792 and NS059348 to J.L., and grant no. NIAID 5RC1AI086152 to J.C.L.), by the Charles A. Dana Foundation (J.C.L.) and by the American Heart Association (grant no. 0970178N to J.M.K.). W.Z. is supported by an International Human Frontier Science Program Organization postdoctoral fellowship. Y.J.Y. holds a National Science Foundation Graduate Fellowship.

Author contributions

W.Z. and J.M.K. are responsible for study concept and design. W.Z., J.M.K., J.L., J.C.L., C.P.L., D.S. and R.K. prepared the manuscript. W.Z., S.S., J.C., Y.J.Y., M.L.L., S.B., A.L.C., J.A.P, W.T., I.A.D. and C.C. carried out experiments and performed data analysis. R.K.J. provided genetically engineered cells.

Additional information

The authors declare no competing financial interests. Supplementary information accompanies this paper at www.nature.com/naturenanotechnology. Reprints and permission information is available online at http://www.nature.com/reprints/. Correspondence and requests for materials should be addressed to J.M.K.

nature nanotechnology

SUPPLEMENTARY INFORMATION

DOI: 10.1038/NNANO.2011.101

Cell surface sensors for real-time probing of cellular environments

Weian Zhao[1,2,3,4], Sebastian Schafer[1,2,3,4], Jonghoon Choi[5], Yvonne J. Yamanaka[5,6], Maria L. Lombardi[7], Suman Bose[8], Alicia L. Carlson[2,9], Joseph A. Phillips[1,2,3,4], Weisuong Teo[1,2,3,4], Ilia A. Droujinine[1,2,3,4], Cheryl Cui[1,2,3,4], Rakesh K. Jain[10], Jan Lammerding[7], J. Christopher Love[5], Charles P. Lin[2,3,9], Debanjan Sarkar[1,2,3,4], Rohit Karnik[8], & Jeffrey M. Karp[1,2,3,4]

Corresponding Author

Jeffrey M. Karp

Co-Director of the Center for Regenerative Therapeutics

Brigham and Women's Hospital,

Room 313, PRB

65 Landsdowne Street

Cambridge, MA 02139, USA

Tel: 617-817 9174

Fax: 617-768-8338

Email: jkarp@rics.bwh.harvard.edu

Materials

All DNA (names and sequences in Table S1) were obtained from Integrated DNA Technologies (IDT). Recombinant PDGF-BB and PDGF-BB ELISA kit were purchased from R&D systems (Minneapolis, MN). Primary human MSCs were obtained from the Center for Gene Therapy at Texas A&M which has a grant from NCRR of the NIH, Grant # P40RR017447. PDGF-BB producing human MDA-MB-231 cells, provided by Prof. Jain at Massachusetts General Hospital, were genetically engineered using retrovirus transduction following a previously established protocol.[1] α-MEM, Fetal Bovine Serum (FBS), L-Glutamine and Penn-Strep were purchased from Invitrogen. Sulfonated biotinyl-N-hydroxy-succinimide (NHS-Biotin), streptavidin, trypsin/EDTA solution, PBS-/- (NaCl 137mM, KCl 26.8mM, Na_2HPO_4 8.1mM, KH_2PO_4 1.5mM) and PBS+/+ (PBS-/- supplemented with 0.9 mM $CaCl_2$ and 0.5 mM $MgCl_2$) were purchased from Sigma.

Mesenchymal Stem Cell Culture and Characterization

Primary human MSCs were isolated from human marrow of healthy consenting donors and thoroughly characterized as previously described before sending to the researchers [2, 3]. Before use, we further confirmed the basic characteristics (i.e. CD90+, CD29+, CD106+, CD34-, CD45-) of MSCs using flow cytometry. MSCs were adherent on tissue culture plate and were maintained in MSC medium that consisted of 15% FBS, 1% (v/v) L-Glutamine, 1% (v/v) Penn-Strep, and α-MEM. To detach cells from plates for passaging or experiments, cells were incubated in 1 × trypsin/EDTA solution at 37 °C for 3 min. MSCs at passage number 4-6 with confluency of ~ 80% were used for all experiments.

Computational model for PDGF transport in microneedle experiment

We built a computational model to estimate the local concentration of the PDGF near the cell. The following simplifying assumptions were made:

1. The flow is determined primarily by the direction and magnitude of injection velocity, and pipette body has minimal effect on the flow profile. This allows us to model the pipette as a thin vertical tube (Figure S6) and the direction of injection (30^o) and magnitude of velocity (100 μm/s) are similar to those used in the experiment.
2. The flow is assumed to be symmetric about the pipette (one vertical plane of symmetry) allowing us to model only half of the computational domain.
3. It is assumed that the cells do not alter the flow pattern appreciably. Thus, we model only one cell (the cell of interest, which was photographed in the micro needle experiment), as a hemispherical cap, in our computational domain.
4. The cell surface concentration of aptamer was assumed to be low such that binding of PDGF on the surface does not appreciable alter the local PDGF concentration.

The computational domain was created and meshed in the commercial software GAMBIT (preprocessor of FLUENT, Ansys Inc.) using tetrahedral elements with edge lengths graded from 1 μm (boundary elements) to 3 μm (elements in the bulk fluid) (Figure S6). The meshed volume was exported into the computational software FLUENT (Ansys, Inc.) and the appropriate boundary conditions were applied (Figure S6). An unsteady incompressible laminar fluid flow model along with non-reacting species transport was chosen. This model uses finite volume method to discretize the continuity, Navier-Stokes and the mass transport equations shown below (gravity was neglected):

$$\nabla\bullet(\rho\vec{\vartheta}) = 0$$

$$\frac{\partial}{\partial t}(\rho\vec{\vartheta}) + \vec{\vartheta}\bullet\nabla(\rho\vec{\vartheta}) = -\nabla P + \mu\nabla^2\vec{\vartheta}$$

$$\frac{\partial C}{\partial t} + \vec{\vartheta}\bullet\nabla C = D\nabla^2 C$$

where ρ is the fluid density, $\vec{\vartheta}$ is the fluid velocity vector in cartesian coordinates, P is the static pressure, μ is fluid viscosity, C is the concentration of the transported species and D is the coefficient of diffusion of the species in the medium. The material properties used in our simulations were: ρ=998.2 kg/m^3, μ= 0.001003 kg/m-s, molecular weight of water = 18.01 Da, molecular weight of PDGF-BB=24.3 kDa, D=1x10^{-10} m^2/s [4]. A segregated solver along with 1st order implicit time stepping method was used. The pressure was discretized using PRESTO scheme while the momentum and species equation used a 2nd order upwind scheme (both are inbuilt options in the software). The injected stream is assumed to have a PDGF mass fraction of 1 (accordingly, the calculated mass fraction of PDGF is interpreted as the concentration relative to the injected value). Unsteady simulations were performed with time step of 0.1 s with a maximum of 50 iterations per time step. The solution was terminated when all the residuals were below 10^{-4}. The initial condition was no flow, and no PDGF present in the geometry (i.e. mass fraction of water is 1). The simulation was run in double precision mode.

PDGF-BB production by MDA-MB-231 cells determined by ELISA

The amount of PDGF-BB produced by genetically engineered or wild-type MDA-MB-231 cells was quantified using an ELISA kit following a protocol provided by R&D Systems. It was determined that PDGF is continuously secreted to a total concentration of ~1.75 nM in 6 h, which falls in the detection range of our cell surface sensors.

Fabrication of microwell

Microwell arrays were prepared by injecting a silicone elastomer mixture (polydimethylsiloxane (PDMS), Dow Corning Inc.) into a mold and curing at 70°C for 2h. The prepared arrays were 1 mm thick and bound to a glass slide. Each array consisted of ~85,000 microwells (each 50 μm × 50 μm × 50 μm) arranged in 7 x 7 blocks. Arrays were treated for 30 s in an oxygen plasma chamber (Harrick PDC-32G) to render the surface sterile and hydrophilic.

Animals and intravital confocal microscopy

All mice were housed according to IACUC guidelines and used for experiments when 6-10 weeks old. Aptamer-modified MSCs (labeled with DiD) and native MSC (labeled with DiO) or FRET probe-modified MSCs (10^6 cells/100 µL PBS) were injected via retro-orbital injection into anesthetized female Balb/C mice. 24 h after the injection, the mice were anaesthetized by an intraperitoneal injection of a Ketamine/Xylazine cocktail at 100 mg/kg / 15 mg/kg body weight and prepared for in vivo imaging by making a small incision in the scalp to expose the underlying dorsal surface of the skull. High-resolution images were acquired through the intact mouse skull of a live mouse using a non-commercial confocal/multi-photon microscope specifically designed for live animal imaging.[7, 8] Circulating blood was stained through delivery of rhodamine-dextran conjugate (Invitrogen, 70kDa) at 10 mg/kg just before imaging. DiO was imaged using 491nm excitation (Dual Calypso, Cobolt AB, Stockholm, Sweden) and 509-547 nm emission (Semrock, Rochester, NY), DiD was imaged using 635nm excitation (Radius, Coherent, Santa Clara, CA) and 667-722 nm emission (Omega Optical, Brattleboro, VT). Rhodamine was imaged using 561 nm excitation (Jive, Cobolt AB, Stockholm, Sweden) and 573-613 nm emission (Semrock, Rochester, NY) whereas collagen in bone was imaged via second harmonic generation using an 880nm incident two-photon laser source (Mai Tai HP, Spectra-Physics, Irvine, CA) and a 432-482 nm bandpass filter (Semrock, Rochester, NY). Z-sections were acquired using 5 um steps. To measure extravasation, fluorescent images from different channels must remain aligned during image acquisition, therefore rhodamine, DiO, and DiD images were acquired simultaneously during z-stack acquisition. Image analysis was performed using ImageJ (NIH, Bethesda, MD). Statistical differences between MSC and aptamer-MSC transmigration were determined using the Fisher exact test.

For experiments where MSCs were labeled with FRET probe, fluorescence images were acquired before and after photobleaching of the FRET acceptor (Cy5). Images were acquired using 532 nm excitation from a solid-state laser (Dual Calypso, Cobolt AB, Stockholm, Sweden) and the Cy3 and Cy5 fluorescence

were detected through a 570-620 nm bandpass filter (Chroma Technologies, Rockingham, VT) and a 650-760 nm bandpass filter (Chroma Technologies, Rockingham, VT), respectively. The frame rate of the microscope was fifteen frames per second. Images were captured, after averaging fifteen frames, using a Macintosh computer equipped with an Active Silicon snapper card (Active Silicon Chelmsford, MA). Each channel was acquired individually, but simultaneously, in 8-bit grayscale and merged to form an RGB image, with Cy3 fluorescence in the green channel and Cy5 fluorescence in the red channel, using custom developed software (iPhoton).

The FRET acceptor, Cy5, was photobleached by illuminating the region of interest (330 x 330 μm) with approximately 3.6 mW of power (measured after the microscope objective) for 3 minutes using a 635 nm helium-neon laser (Radius, Coherent Inc., Santa Clara, CA).

Table S1. Names and sequences of DNA molecules used in this study.

Names	Sequences (5'->3')
Quench-FAM	FAM-AAG GCT ACG GCA CGT AGA GCA TCA CCA TGA TCC TGT GTG GTC TAT GTC GTC GTT CG
Quench-Dabcyl	Biotin-CGA ACG ACG ACA TAG ACC ACA-Dabcyl
Quench-Cy5	Cy5- AAG GCT ACG GCA CGT AGA GCA TCA CCA TGA TCC TGT GTG GTC TGT GTC G
Quench-IBRQ	Biotin-CGA ACG ACG ACA TAG ACC ACA-Iowa Black RQ
FRET-Cy5	Cy5-AAG GCT ACG GCA CGT AGA GCA TCA CCA TGA TCC TGT GTG GTC TGT GTC G
FRET-Cy3	Biotin-CGA CAC AGA CC/Cy3/A CA
FRET-probe	Cy3-TT-Cy5-TTTTTTTT-Biotin

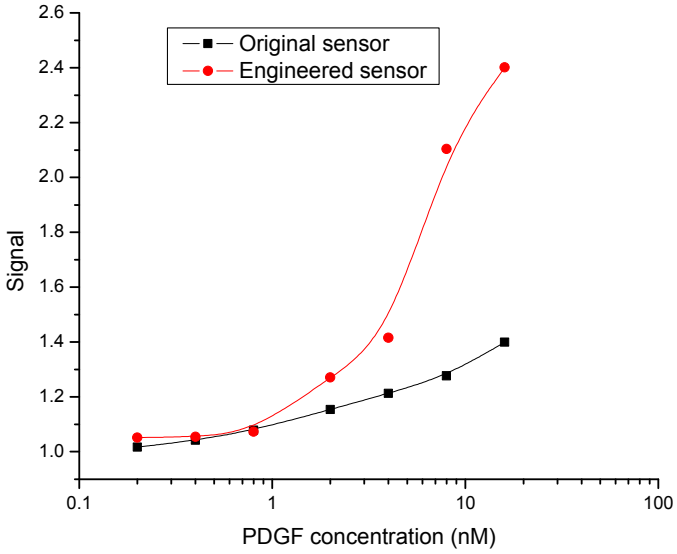

Figure S1. Performance of original and engineered PDGF sensor in solution (PBS+/+). The sensor was engineered by changing a C-G base pair to A- -G non base pair. Y axis represents the signal that is defined as the ratio of fluorescence, obtained by flow cytometry, before and after addition of PDGF. 10 nM sensor molecules were used in this experiment and spectra were recorded immediately at room temperature.

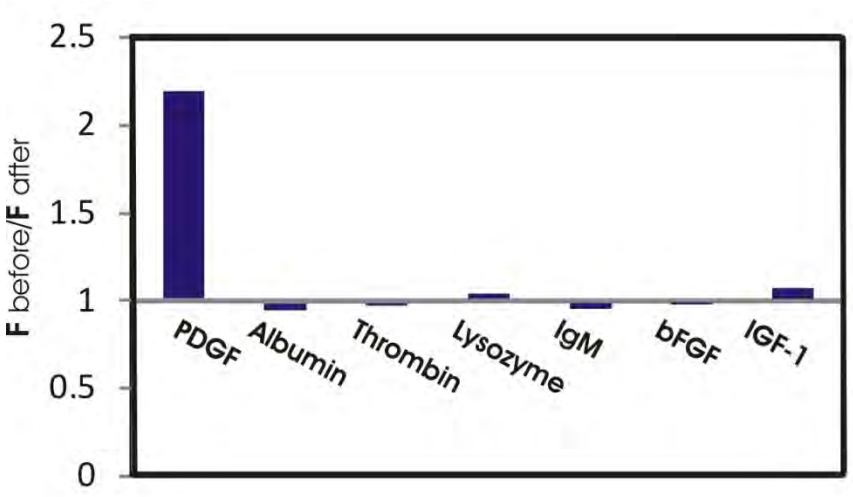

Figure S2. Binding specificity of the PDGF aptamer sensor on the MSC surface. Y axis is the ratio of fluorescence signal (at 520 nm) before and after adding tested molecule (20 nM in PBS). bFGF: basic fibroblast growth factor; IGF-1: insulin-like growth factor-1.

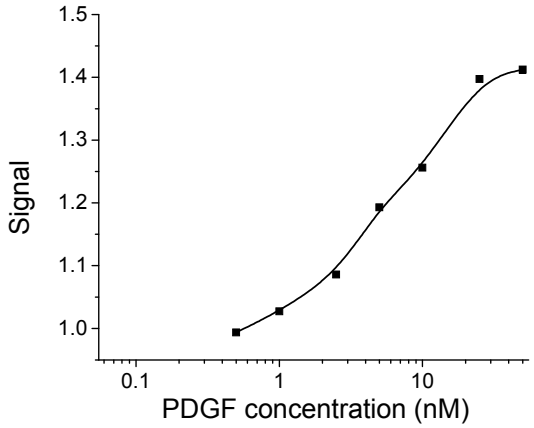

Figure S3. Calibration curve of the FRET sensor on the MSC surface for quantifying PDGF concentration. Signal is defined as the fluorescence decrease of donor dye (Cy3) × fluorescence increase of acceptor dye (Cy5) on MSC at a particular PDGF concentration. Each signal value (y-axis) represents the average

fluorescence intensity from ~ 60 individual cells imaged by fluorescent microscopy at 37°C in PBS-/-. FRET sensor modified MSCs were excited by a 568 nm laser and emissions were measured at 607 nm and 670 nm for Cy3 and Cy5, respectively.

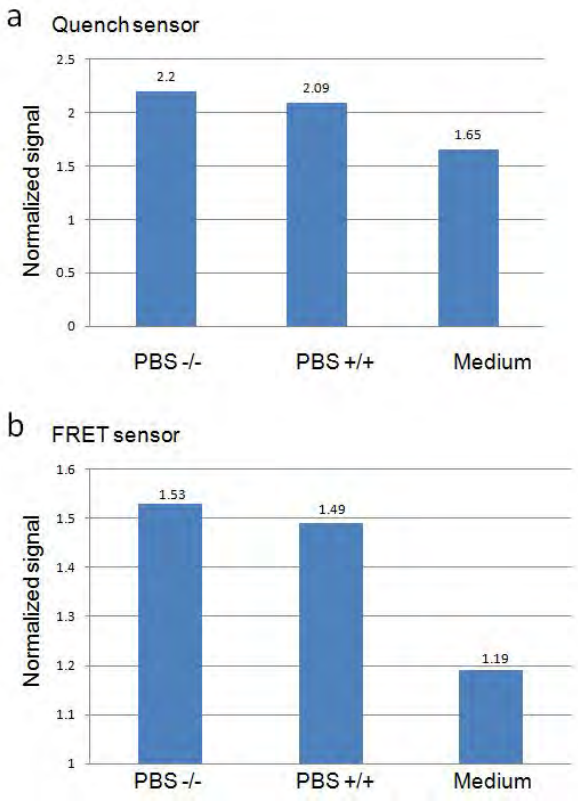

Figure S4. (a) Performance of the quench sensor and (b) FRET sensor immobilized on the MSC surface in different solution. Medium contains 15% FBS, 1% (v/v) L-Glutamine, 1% (v/v) Penn-Strep, and α-MEM. Signal for the quench sensor is defined as the ratio of geometric means of the flow cytometry histogram before and after addition of PDGF. Signal for the FRET sensor is defined as the fluorescence decrease of donor dye (Cy3) × fluorescence increase of acceptor dye (Cy5) based on the geometric means in the flow cytometry histogram. 20 nM PDGF was used and measurement was performed immediately at room temperature.

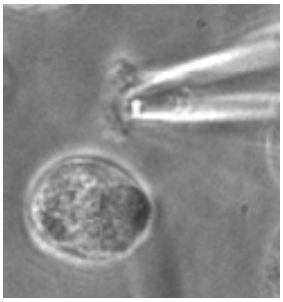

Figure S5. A representative example how PDGF was injected by microneedle.

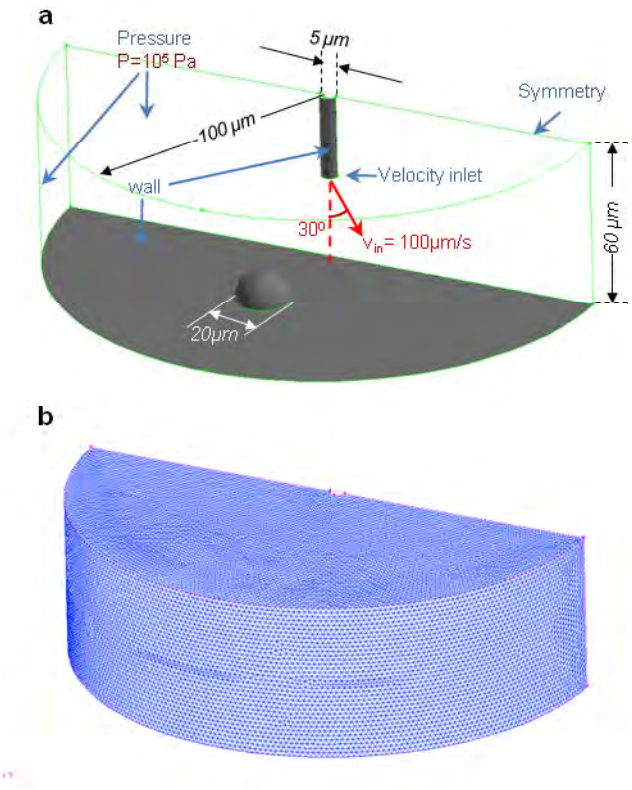

Figure S6: Modeling of PDGF concentration around the sensor-cell. a) Computational domain used for modeling the PDGF transport in the microneedle experiment. The boundary conditions are shown (blue text) along with their values (red text). The dimensions are also shown. Note that the flow is determined primarily by the direction and magnitude of injection velocity, and pipette body has minimal effect on

the flow profile. This allows us to model the pipette as a thin vertical tube (a) and the direction of injection (30^{o}) and magnitude of velocity (100 µm/s) are similar to those used in the experiment. b) Discretized computational domain showing the tetrahedral elements used for meshing.

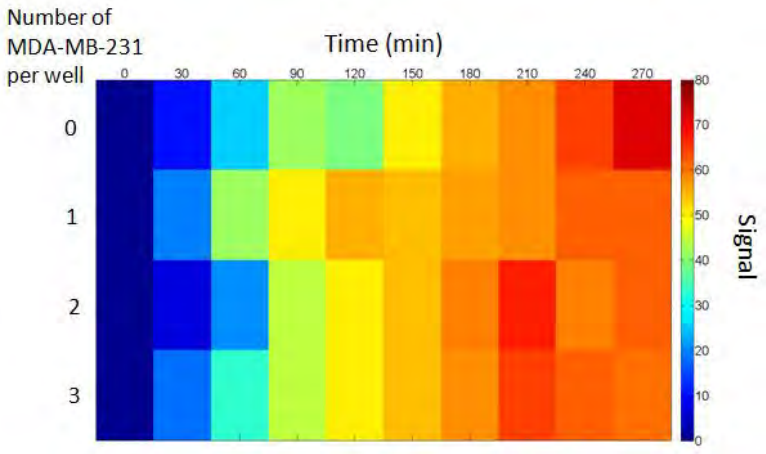

Figure S7. No significant signal difference on sensor-MSCs in the presence and absence of non-genetically engineered MDA-MB-231. The signal is defined as the percentage of MSCs that have fluorescence intensity less than 50% of their initial value at the indicated time. Note that the fluorescence intensity of the quench sensor on the cell surface may be influenced by external factors including the sensor site density per cell and medium conditions including pH, temperature, and composition, which may explain the difference observed in the overall fluorescence quenching between this experiment and the experiment reported in Figure 5.

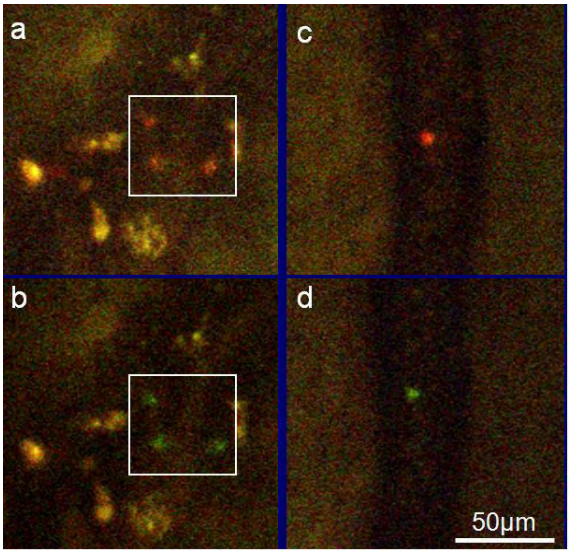

Figure S8. Representative in vivo IVM images of FRET-probe-modified MSCs that homed to the skull bone marrow in the live mice. Images were taken 24 h after systemic infusion of cells via retro-orbital injection. a, c and b, d are images acquired before and after in situ photobleaching of Cy5, respectively. Cy3 fluorescence was acquired in the green channel and Cy5 fluorescence was acquired in the red channel. Scale bar is 50 µm.

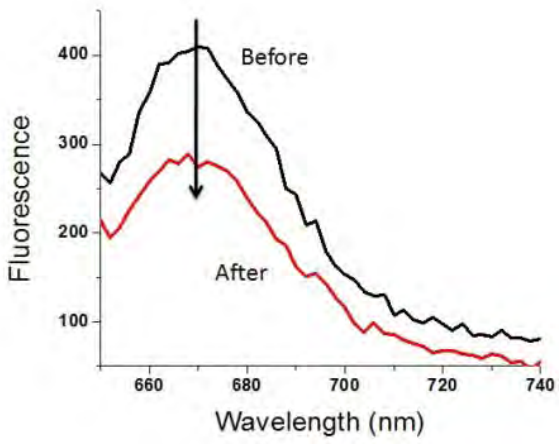

Figure S9. The performance of the quench sensor using Cy5/Iowa Black RQ before and after addition of PDGF (10 nM) in PBS-/-.

References

1. Au, P. et al. Paradoxical effects of PDGF-BB overexpression in endothelial cells on engineered blood vessels in vivo. *The American Journal of Pathology* **175**, 294-302 (2009).
2. Sekiya, I. et al. Expansion of human adult stem cells from bone marrow stroma: Conditions that maximize the yields of early progenitors and evaluate their quality. *Stem Cells* **20**, 530-541 (2002).
3. Sarkar, D. et al. Chemical Engineering of Mesenchymal Stem Cells to Induce a Cell Rolling Response. *Bioconjugate Chemistry* **19**, 2105-2109 (2008).
4. Haugh, J.M. Deterministic model of dermal wound invasion incorporating receptor-mediated signal transduction and spatial gradient sensing. *Biophysical Journal* **90**, 2297-2308 (2006).
5. Ogunniyi, A.O., Story, C.M., Papa, E., Guillen, E. & Love, J.C. Screening individual hybridomas by microengraving to discover monoclonal antibodies. *Nature Protocol* **4**, 767-782 (2009).
6. Han, Q., Bradshaw, E.M., Nilsson, B., Hafler, D.A. & Love, J.C. Multidimensional analysis of the frequencies and rates of cytokine secretion from single cells by quantitative microengraving. *Lab Chip* **10**, 1391-1400 (2010).
7. Runnels, J.M. et al. Imaging molecular expression on vascular endothelial cells by in vivo immunofluorescence microscopy. *Mol Imaging* **5**, 31-40 (2006).
8. Celso, C. et al. Live-animal tracking of individual haematopoietic stem/progenitor cells in their niche. *Nature* **457**, 92-97 (2009).